JAAS

Journal of Analytical Atomic Spectrometry

www.rsc.org/jaas

Volume 28 | Number 8 | August 2013 | Pages 1133–1356

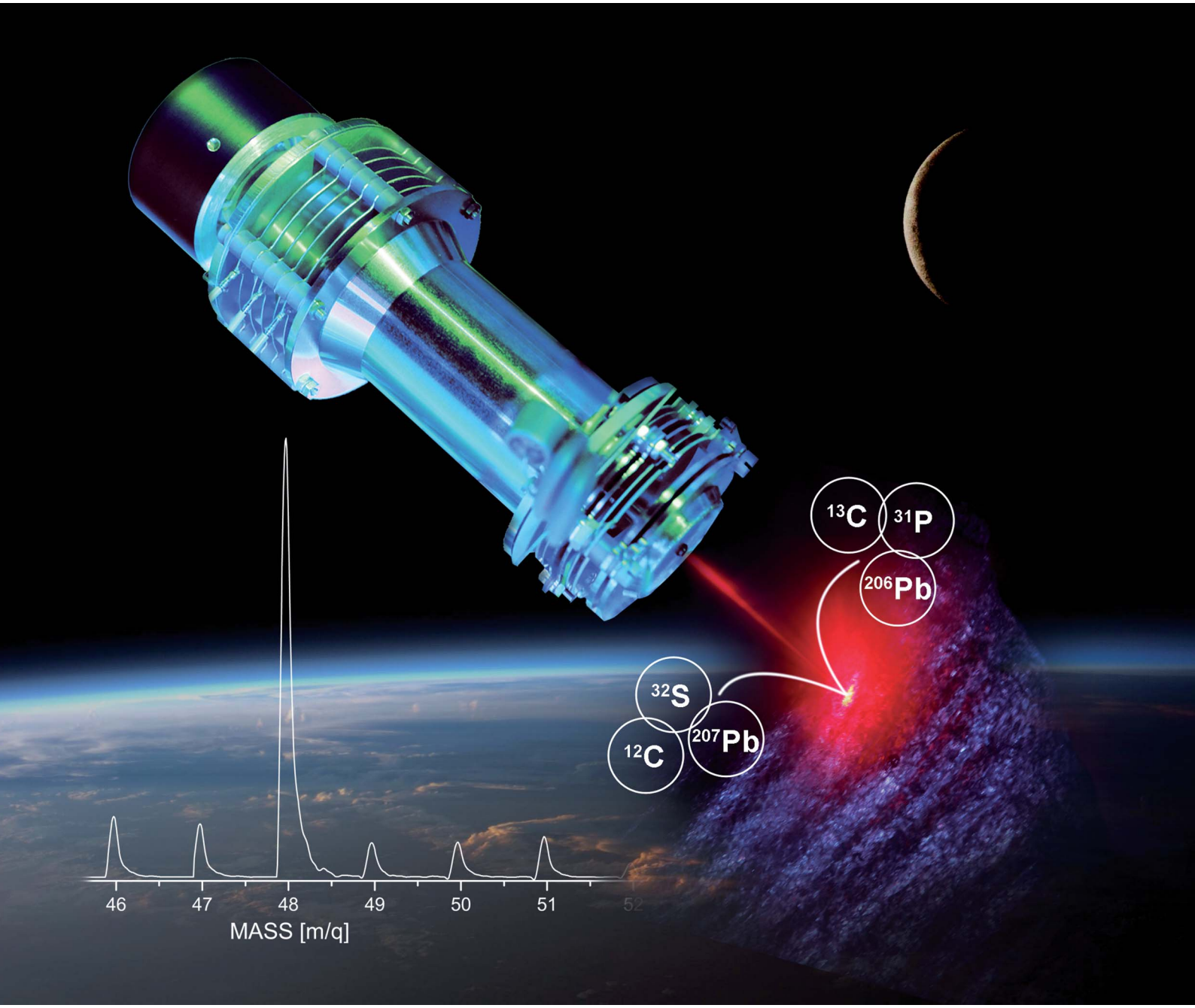

ISSN 0267-9477

RSC Publishing

PAPER

Andreas Riedo *et al.*

Coupling of LMS with a fs-laser ablation ion source: elemental and isotope composition measurements

JAAS

RSC Publishing

PAPER

View Article Online
View Journal | View Issue

Coupling of LMS with a fs-laser ablation ion source: elemental and isotope composition measurements

Cite this: *J. Anal. At. Spectrom.*, 2013, **28**, 1256

Andreas Riedo,* Maike Neuland, Stefan Meyer, Marek Tulej and Peter Wurz

Mass spectrometric analysis of elemental and isotopic compositions of several NIST standards is performed by a miniature laser ablation/ionisation reflectron-type time-of-flight mass spectrometer (LMS) using a fs-laser ablation ion source (775 nm, 190 fs, 1 kHz). The results of the mass spectrometric studies indicate that in a defined range of laser irradiance (fluence) and for a certain number of accumulations of single laser shot spectra, the measurements of isotope abundances can be conducted with a measurement accuracy at the per mill level and at the per cent level for isotope concentrations higher and lower than 100 ppm, respectively. Also the elemental analysis can be performed with a good accuracy. The LMS instrument combined with a fs-laser ablation ion source exhibits similar detection efficiency for both metallic and non-metallic elements. Relative sensitivity coefficients were determined and found to be close to one, which is of considerable importance for the development of standard-less instruments. Negligible thermal effects, sample damage and excellent characteristics of the fs-laser beam are thought to be the main reason for substantial improvement of the instrumental performance compared to other laser ablation mass spectrometers.

Received 1st April 2013
Accepted 29th May 2013

DOI: 10.1039/c3ja50117e

www.rsc.org/jaas

Introduction

The development of miniature mass spectrometers is of considerable interest for a variety of field applications but also for their use on space missions for planetary space research. In particular, the investigation of elemental and isotopic compositions of solid materials by mass spectrometric methods has become promising with developments of miniature laser ablation/ionisation mass spectrometers.[1–4]

The development of space instrumentation capable of sensitive measurements of elements and their isotopes is of considerable interest to current cosmochemistry and planetology, and drives current instrument development. The knowledge of the isotopic composition and its variation in planetary materials, soils/regolith and rocks is important for establishing critical constraints in models of the origin and evolution of our solar system. Current planetary material is a product of a number of physical and chemical processes that modified the presolar chemical mixture during the solar system evolution. Formation of first solids, mixing, melting and crystallisation, geochemical processes and interaction of a planetary surface with cosmic or solar radiation led to large elemental composition changes. However, isotopes of chemical elements are found to be robust tracers of pre-solar events and processes and their changes over the planetary evolution time are relatively small.[5–8] The measurements of the element abundances and isotope patterns of planetary surface material impose critical constraints on event chronology in the early stages of solar system formation and help to constrain the time of formation of planetary material (crystallisation ages). Accurate measurements of elemental and isotopic fractionation effects of various classes of elements (volatile/non-volatile, geochemically relevant, bio-relevant, radiogenic) can yield information on the conditions and differentiation processes operating on a planetary surface.[5,6,9] The determination of time scale and insight into timing of various rock-forming processes and detailed understanding of the chronology of the early solar system can be performed by radio-isotope chronology of planetary material. The method requires precise and accurate measurements of isotope ratios (*e.g.*, Pb isotopes for the Pb/Pb-dating method). Such measurements are extremely challenging and until now, they have not been attempted in space research because of the lack of suitable instrumentation for use on spacecraft. Gas phase analyses using space instruments such as Ptolemy on Rosetta should have the capability of achieving an analytical precision of about 5‰ or better and the Gas Analytical Package (GAP) on Beagle 2 of about 1‰ or better for isotope ratios.[10–13] However, current space instrumentation designed for investigations of the chemical composition of solid materials allows the measurement of major and minor elements with elemental concentrations in sample material at best at the per mill level.[14–19] More sensitive instruments are necessary in space research. A few prototype instruments are considered for space research.[3,4,20–22] Among other methods, laser ablation/ionisation

Physics Institute, Space Research and Planetary Sciences, University of Bern, Sidlerstrasse 5, 3012 Bern, Switzerland. E-mail: andreas.riedo@space.unibe.ch; Fax: +41 31 631 44 05; Tel: +41 31 631 44 49

mass spectrometry (LIMS) is currently a very promising method that can be applied for sensitive, accurate and precise elemental and isotope *in situ* analyses in space research. Albeit, the investigation of isotope composition in the laboratory is conducted mainly by other mass spectrometric techniques, such as inductively coupled plasma mass spectrometry (ICP-MS), thermal ionisation mass spectrometry (TIMS), or secondary ionisation mass spectrometry (SIMS),[23] recent developments in LIMS show that this method can be also very sensitive and has the potential of delivering highly accurate and precise measurements.[22,24,25]

LIMS is a truly sensitive mass spectrometric technique. So far, it has been less commonly used for isotope composition measurements and it has been considered for some time only as a semi-quantitative method for the element and isotope abundance determination.[26,27] In particular, the measurements of the isotopic patterns were reported to have accuracy and precision at the per cent level in contrast to laser ablation ICP-MS and TIMS methods.[23] LIMS has, however, still the potential for improvement and with the recent progress in laser technology, fast electronics, and improved vacuum technology, this technique becomes attractive in chemical analysis of solid samples.[25,28–30] Recent studies show that LIMS can be used for highly accurate investigation of the elemental composition as well as for isotopic concentration measurements with high accuracy and precision.[22,24,25,28–34] Typically, only femtograms to picograms of sample material are needed for sensitive investigation with high lateral and vertical resolution of sample composition.[24,32,35,36] Similar to other analytical methods, LIMS requires a proper calibration before conducting quantitative analyses. The physical and chemical properties of a sample, choice of a laser ablation ion source and calibration constants are found to be the main reasons for low performance of measurements.[37] According to very recent developments, however, the method can be considered under certain experimental conditions as standard-less.[38–41] The present studies attempt to define experimental conditions under which LIMS becomes very sensitive and allows quantitative investigations with high accuracy and precision by using a fs-laser ablation ion source.

Our primary goal is to develop a miniature LIMS technique for application in space research. LIMS has many advantages over the LA-ICP-MS, TIMS and SIMS techniques. The latter techniques are more difficult to adopt for space research where a high degree of miniaturisation, low mass and volume, and low power consumption for operation are required. LIMS instruments can be robust, and easily fulfil space requirements. A few such instruments were developed in the last two decades, *e.g.*, LASMA, LAMS, and LMS.[1–4] A number of studies on the instrument performance showed that miniaturised LIMS systems can be highly sensitive delivering the measurements of all chemical elements with detection limits at the level of ~10 ppb.[22] In contrast to previous reports,[14] our and other recent studies showed that a LIMS system including the LMS instrument[22,34] is capable of conducting measurements on isotope compositions within a measurement accuracy at the per mill and sub per mill levels.[25,42]

In analytical chemistry, laser ablation experienced major progress in the last few years by the implementation of ultra-short pulsed laser systems.[35,36,43–48] Ultra-short laser pulses <1 ps are of particular interest for laser ablation of sample material, because the pulse duration is shorter than the characteristic time typical for the phase transition from the solid to hot plasma plume that is produced above the sample surface and laser–plasma interaction can be avoided.[36,46] Several processes taking place during the ablation, including thermalisation of the deposited laser energy (lattice relaxation time), the explosive release of vapour, and formation and cooling of a plasma plume that is additionally heated by laser radiation are the main sources of elemental fractionation effects.[43,44] Due to reduced thermal diffusion depth high geometric precision in the laser ablation and minimal collateral sample damage can be obtained using short laser pulses.[36,44,46,48] Moreover, the laser beam does not interact with the laser-induced plasma due to its short pulse duration.[43,44,46] The absorbed laser energy is fully deposited into the sample material and higher efficiency of material ablation can be obtained.[46]

Recent investigation with our miniature laser ablation/ionisation time-of-flight mass spectrometer with a ns-laser ablation ion source showed its potential for accurate measurement of isotope patterns with accuracy at the per mill level.[22] In this study we use a similar measurement procedure to that applied in our previous studies with a ns-laser ablation ion source.[34] NIST standard reference materials were used to investigate the accuracy and precision of the measurement of the elemental/isotopic composition. The results are compared to those measured with an ns-laser ablation ion source.

Experimental

The details of the technical design and principles of operation of the LMS instrument were described in previous publications.[1,22,28,31,32,34] Thus, only a brief overview of the experimental setup with its update will be given here. While in previous studies nanosecond laser systems were used for ablation and ionisation of sample material,[1,22] in the present study a femtosecond laser ablation ion source is used.

Experimental setup and principle of operation

Fig. 1 shows the image of the current laboratory system: (A) the computer control station, (B1/B2) electronics, including power supplies, data acquisition systems, vacuum system controls, *etc.*, and (C) the instrument setup itself with all the details shown in Fig. 2.

The laboratory is kept at clean room conditions (ISO 5, Class 100) by a laminar flow ceiling to protect the laser systems, their optics, the samples, vacuum chambers, *etc.*, from possible dust and particles inside the laboratory. A constant overpressure relative to the outside is maintained, the temperature of the laboratory is kept at (22.0 ± 0.4) °C, and the humidity is controlled at (42.0 ± 0.5)° relative humidity level. All parameters are monitored continuously and displayed in a web interface.

Fig. 1 Overview of the instrument setup in the laboratory. (A) represents the remote control station; (B1/B2) the electronic equipment, *e.g.* measurement computer, power supplies, *etc.*; (C) the instrument setup itself. Detailed information about part (C) can be found in Fig. 2.

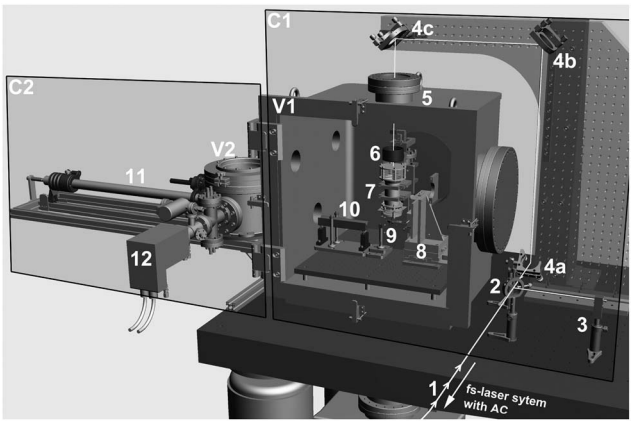

Fig. 2 Technical drawing of the instrument setup shown in Fig. 1 as part C. (C1) fs-laser beam optical setup: (1) laser beam, autocorrelator and first beam splitter are in front of the setup, (2) second beam splitter, (3) ultrafast photodiode, (4a–c) dielectric laser mirrors; (5) entrance window into the vacuum chamber, (6) beam focusing lens, (7) mass analyser with detector, (8) *x*, *y*, *z* micro-translation stage, (9) sample holder, (V1) main vacuum chamber. C2: (10 and 11) sample exchange and transport system, (12) argon sputter gun, and (V2) sample port vacuum chamber.

These clean room conditions guarantee stable operational conditions for the equipment.

Fig. 2 displays a technical drawing of the LMS system (part (C) shown in Fig. 1) with a fs-laser ablation ion source. The LMS instrument is accommodated in the main UHV chamber (V1) and the sample introduction/transport system in the smaller UHV chamber (V2). The base pressure in both UHV systems is typically in the low 10^{-8} mbar range, and is realised with turbomolecular pumps in each system and an additional ion getter pump for V1. During measurement campaigns both turbomolecular pumps are switched off and only the ion-getter pump is running. This procedure ensures vibration-free conditions.

An argon ion sputter gun (tectra GmbH, Physikalische Instrumente, Germany) is installed at V2 and is used to clean the sample surface from a possible surface contamination, if necessary. High purity argon gas is typically used for the cleaning process (Carbagas, Switzerland). The argon gun is operated typically at 3 keV, but ion beam energies can be tuned from hundredths of eV to 5 keV. The angle of incidence of the incoming argon ions relative to the sample surface is $\sim 10^{\circ}$.

Samples are introduced with the sample transport system (10, 11) from V2 to V1 and positioned just below the entrance electrode of the mass analyser, on a sample holder (9), which is attached to the *x*–*y*–*z* micro-translational stage (8). The accuracy of sample positioning and step resolution of these translational stages is ~ 2 μm. The distance between the sample surface and the entrance of the instrument is about 1 mm, which corresponds roughly to the laser focus location. There is no contact between the sample surface and the entrance plate to avoid possible sample contamination.

Short laser pulses ($\sim$190 fs, $\lambda = 775$ nm) produced by a Ti–Sapphire femtosecond laser system (CPA system, Clark-MXR Inc., USA) are used to ablate and ionise surface material. The repetition rate (up to 1 kHz), laser pulse energy (up to 1 mJ), and the number of laser shots were controlled remotely *via* a measurement computer.

Small fractions of the laser beam are reflected from two beam splitters for *on line* measurement of pulse duration by an autocorrelator system (AC, PulseChek, APE GmbH, Germany) and of the laser intensity by an ultrafast Si-photodetector (Alphalas GmbH, Germany) (5), respectively. The data measured using the autocorrelator are transferred directly to a computer, whereas the Si-photodetector signal is measured with an ADC card.

The laser beam is guided *via* a set of dielectric mirrors (4a–c) to the optical port of the vacuum chamber V1 and enters the mass spectrometer along its ion-optical axis. The laser radiation is focused subsequently by a lens ($f = 200$ mm, NA = 4) (6), which is positioned directly above the ion mirror, onto the sample surface to a spot size of about 40 μm after passing the entrance window on the reflectron, the central hole (Ø 6.4 mm) of the detector assembly, and the ion-optical elements of the ion confinement (Fig. 3). The material ablated from the sample surface forms a hot plasma plume consisting of atomised and ionised species. Close proximity of the plasma plume to the entrance of the mass analyser allows a major fraction of positive ions to enter the mass analyser through the conical extraction electrode. After entering the interior of the mass analyser, ions are guided by electrical fields towards the detector. After initial acceleration, focussing and collimation by an electrostatic immersion lens, the ions fly through the field-free region (drift tube) and ion mirror (reflectron) where they are eventually reflected and guided towards the multichannel plate (MCP) ion detector. A pair of MCPs arranged in a chevron configuration is used to generate the electric signal on the anode after the ions strike the MCPs. The MCP detector can be operated at gains of up to 10^8. The ions arrive at the MCP detector in a sequence of times proportional to the square root of their mass-to-charge ratio (m/q). The electron current generated by the MCP plates is collected on four concentric anode rings and registered with two high speed ADC data acquisition cards, each with two channels.

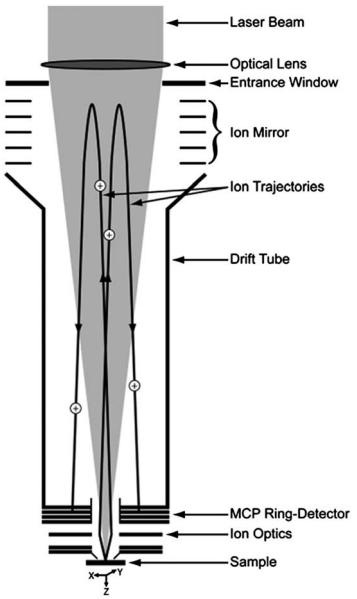

Fig. 3 A schematic drawing of an LMS with a brief overview of the principle of the instrument operation (see also (7) in Fig. 2). The laser beam enters from the top along the ion-optical axis and after being focussed by a lens passes the TOF mass analyser, detector and ion optical system until the beam reaches the sample. The ions produced during the ablation/ionisation process enter the mass analyser and are confined, accelerated, focussed and directed towards the detector by an ion optical system. The mass separation of the ions occurs in the field free region according to their time-of-flight.

The laser firing system is remotely controlled *via* the measurement computer. The laser system electronics generates for each laser pulse two trigger signals, which are forwarded to a high precision multi-channel digital delay generator (DG535 system, Stanford Research Systems, USA) and the autocorrelator system. The delay generator triggers subsequently two ADC cards and hence starts the data acquisition (see Fig. 4). A measurement cycle is initiated at the moment when focused laser radiation interacts with the sample surface and produces ions. Two high speed ADC cards, one PCI (U1082A, AP240 with average firmware, Agilent) and one PCIe (U1084A, Agilent) card, are used for data acquisition. Each card has two input channels with a vertical resolution of 8 bits for a single shot. The PCI card supports a sampling rate of 1 GS s^{-1} with an analogue bandwidth of 1 GHz for each channel, whereas the PCIe allows a sampling rate of 2 GS s^{-1} with an analogue bandwidth of 1.5 GHz for each channel. For each card, these two channels can be combined into one channel with a doubled sampling rate of 2 GS s^{-1} and 4 GS s^{-1}, respectively. In the present measurements one channel of the PCI card is used to measure the signal from the ultrafast Si-photodetector and the other three channels to measure the signals collected from three of the four anode rings.[1,22] To protect the anode plate from possible charging effects, the fourth anode ring is short-circuited with 50 Ω outside V1. The measurements are performed by collecting a number of time-of-flight (TOF) spectra from one sample location. The ADC cards acquire the spectra, store them on the measurement computer and after accomplishment of the measurement campaign, the dataset is subsequently forwarded from the measurement computer to a database on a server. Subsequent data processing is realised on a high performance computer, which is connected directly with the data server. In-house designed analysis software is used for spectra analysis.[22,34] The TOF spectra are measured within a 20 μs time window defined by settings of the acquisition card. This time window allows us to measure mass spectra of elements within a mass-to-charge range of ~600 m/q.

The choice of voltage set for the ion optics and the control of laser ablation conditions including laser fluence and laser irradiance levels, laser focusing geometry and distance between the sample and the entrance to the instrument are crucial parameters for quantitative measurements with a high spatial resolution. Before starting experimental campaigns, the instrument performance is optimised using the procedure described in detail previously.[22,49,50] This procedure optimises a merit function including the ion transmission and mass resolution $m/\Delta m$. Typically, a mass resolution in the range of $m/\Delta m = 500$–700 for the ^{56}Fe mass peak is achieved.[22] More information about the performance optimiser is given in previous publications.[22,49,50]

Samples

Mass spectrometric studies of isotope compositions of different elements, *e.g.* B, Si, P, S, Ti, *etc.*, were performed by using unprocessed National Institute of Standards and Technology (NIST) standard reference materials (SRM) for electrolytic iron

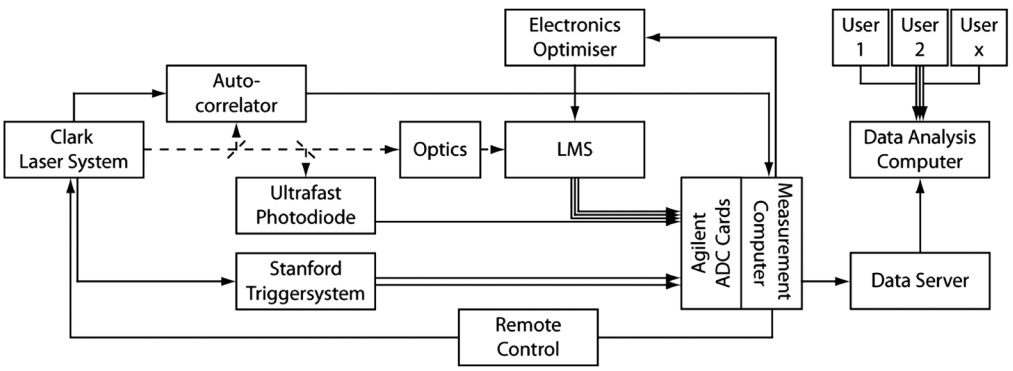

Fig. 4 Functional block diagram of the LMS system (see text for details).

(SRM 661), carbon iron (SRM 664), and steel (SRM 665). Because only elemental abundances are quoted by NIST in these three reference materials terrestrial isotope abundances were assumed in the analysis.[23] The highest possible homogeneity of sample material is guaranteed by NIST. Also sufficiently large surface area was ablated ($Ø \sim 40$ μm) that possible material heterogeneity plays a negligible role in the quantitative analysis (with an exception of the uppermost surface layers which can suffer from oxidation or other contaminations). More details about micro-homogeneity in sample material can be found in the report by Marinenko *et al.*, 1979.[51]

Measurement procedure

The measurement procedure used for accurate isotope composition measurements is described in a previous publication.[34] To achieve stoichiometric ion production, high measurement sensitivity and sufficiently high instrumental performance, both, a laser ablation ion source and mass analyser have to be operated under specific experimental conditions, which are defined by a number of parameters. In particular, for the stoichiometric production of ions the laser ablation ion source has to be operated at specific laser power density (irradiance), with appropriate wavelength, repetition rate and pulse duration. Hence, a choice of laser focus position with respect to sample, laser focussing conditions, laser beam characteristics (temporal and spatial profile) can be critical and can be sometimes difficult to control without a well-defined experimental procedure. Similarly, the conditions for ion confinement, focussing and detection are controlled by ion-optical voltage settings which control ion transmission and mass dispersion. High reproducibility of our measurements is achieved by careful control of a number of parameters and is possible by a computer control routine. This is also used to perform fast check of the experimental performance.[22,49,50]

Each measurement campaign was performed on an untreated sample surface.

(i) *Optimisation of the mass resolution and ion transmission of the instrument.* Mass resolution ($m/\Delta m$) for TOF analysers increases with the ion mass to some extent. Previous studies demonstrated this relationship for the LMS instrument.[22] Albeit LMS can perform the mass spectrometric studies with a mass resolution ($m/\Delta m$) exceeding 1000 at ^{56}Fe (at irradiances < 0.1 GW cm^{-2}), with an increase of the ion production by a laser ablation ion source space charge and ion beam jitter effects start to limit the mass resolution. Nevertheless, the quantitative investigation can be performed with a mass resolution ($m/\Delta m$) in the range 500–700 [22,34]. The optimisation of the mass resolution and ion transmission of the mass analyser is performed by tuning voltage settings on the mass analyser while conducting laser ablation of the surface material under the given experimental conditions (fixed laser spot-sample distance, specific laser fluence). In the current study, the mass analyser performance is a compromise by tuning the mass resolution to about 500 and maximising the ion transmission. Thus, the mass peaks of chemical elements are well separated from each other although the isobaric interferences cannot be removed. For analysis only ion mass peaks were selected for which no isobaric interferences are expected. The dynamic range of the instrument exceeds 10^8 which allows for the detection of trace elements abundant at ppb levels.[22]

(ii) *Choice of the number of accumulated spectra.* The investigation is performed by successive collection of a number of TOF spectra. Each such spectrum is obtained by summing up 2000 single laser shot spectra from the same laser spot. Thus, this dataset allows check on the measurement conditions and the ablation process by monitoring the temporal evolution of ion abundance, cumulative sum of ion signal (integrated mass peak) as well as a survey of the quality including signal-to-noise ratio (SNR), mass resolution ($m/\Delta m$), and relative isotope accuracy of measurement defined as abs ($\text{ratio}_{\text{ref}} - \text{ratio}_{\text{meas}}$)/$\text{ratio}_{\text{ref}}$. The temporal analysis of the spectra is also important for the investigation of sample homogeneity, determination of the influence of surface effects (oxides, possible contamination), and laser repetition rate on the overall quantitative elemental and isotopic analysis of the sample material that can be performed by LMS.[22,31,34]

(iii) *Choice of applied laser irradiance.* The production of ions by a laser ablation ion source depends critically on laser irradiance (laser power density). The systematic studies in a range of applicable laser irradiances were performed with a similar procedure to in (ii). Since the laser focussing conditions (laser beam diameter, sample surface–laser focus distance) were the same, only laser fluence was varied. These studies define the laser irradiance (fluence) for conducting the quantitative elemental (isotope) analysis. The studies yield also the element-specific ablation thresholds.

In-house designed software, written in Matlab, is used for detailed analysis of mass spectra, *e.g.* time-of-flight mass calibration, integration of ion signal (ion mass peak areas), SNR, mass resolution ($m/\Delta m$), relative isotope accuracy of measurement, *etc.*[34,52] Because peak-fitting algorithms, such as Gaussian-fit, showed too high analysis errors (asymmetry of detected mass peaks) we used a direct integration method (Simpson integration) for calculation of ion signal.[34,52] For integration of ion mass peak signal, calculation of isotope accuracy of measurements respectively, no corrections of mass fractionation effects were necessary. In the analysis, the SNR is defined as the ratio of the maximum amplitude of the analysed peak divided by the standard deviation of spectral noise within a range of 1 m/q that is analysed in an area of the spectrum where no mass peaks are detected. Detailed discussion about the analysis software, *e.g.* ion signal integration methods, background correction techniques of mass spectra, *etc.* can be found in the report by Meyer, 2013.[52]

Case study: NIST 661, NIST 664 and NIST 665

A NIST 661 sample was chosen for the analysis of the temporal evolution of the spectral parameters, ion rate production and stability of the laser ablation process. The studies were performed by applying 500 000 laser shots at a laser irradiance of about 1900 GW cm^{-2} (pulse energy of ~4.4 μJ, laser beam diameter: $Ø$ 40 μm) and 250 spectra, each an accumulation of

2000 single laser shot spectra were acquired. SNR, mass resolution ($m/\Delta m$), relative isotope accuracy of measurement, relative peak area error, and cumulative sum of integrated peak areas of different isotopes of different elements, *e.g.* ^{30}Si, ^{32}S, ^{48}Ti, *etc.*, were histogramed and analysed for spectral accumulations of 2000, 4000, …, 400 000 single laser shots. The abundance of elements in the sample are given in weight%-fractions by NIST. For further analysis the NIST quoted elemental concentrations in weight%-fractions were converted to elemental abundances in atomic fractions.[22,28,34] The isotope abundances were calculated by assuming terrestrial isotope ratios.[23]

We find that to perform quantitative measurements of isotope abundance with the highest precision, the spectra obtained from (a) excluding the first 20 000 single laser shots and (b) including the following 100 000 laser shots are optimal (in total 120 000 single laser shots). In the following, 12 measurement campaigns parameterised by energy/pulse in the range of about 1.1–6.2 μJ (~500–2700 GW cm^{-2}) were finally conducted.

Studies on NIST 664 and NIST 665 were performed by employing the same accumulation of spectra, and by applying the laser irradiances in the range that yielded the most accurate measurements for the SRM 661 sample. On each sample, NIST 664 and NIST 665, five campaigns parameterised by laser irradiances were performed to establish the reproducibility of the results and possible dependences on sample surface morphology and composition. Because the samples NIST 664 and NIST 665 are quoted as standards for elemental composition, the isotope composition in the samples is calculated assuming terrestrial isotope ratios.[23] Table 1 gives an overview of the investigated elements/isotopes and their corresponding abundances (in weight and atomic fractions).

Table 1 Elemental abundances of metallic and non-metallic elements as specified for NIST SRM 661, SRM 664, and SRM 664 (second column). The isotope composition was calculated assuming terrestrial isotope ratios,[23] in weight fractions [ppm] (third column). Elemental and isotope abundances in atomic fractions [ppm] are given in the fourth and fifth columns

Element	Weight fraction element [ppm]	Weight fraction isotope [ppm]	Atom fraction element [ppm]	Atom fraction isotope [ppm]
NISR SRM 661				
C	3920.0	^{12}C: 3878.06, ^{13}C: 41.94	17941.4	^{12}C: 17749.42, ^{13}C: 191.97
Si	2230.0	^{29}Si: 104.48, ^{30}Si: 68.95	4364.8	^{29}Si: 204.49, ^{30}Si: 134.96
Ti	200.0	^{46}Ti: 16.50, ^{47}Ti: 14.88, ^{49}Ti: 10.80	229.7	^{46}Ti: 18.95, ^{47}Ti: 17.09, ^{49}Ti: 12.41
Cr	6900.0	^{52}Cr: 5781.44, ^{53}Cr: 655.57	7294.9	^{52}Cr: 6112.29, ^{53}Cr: 693.08
Zr	90.0	^{90}Zr: 46.31, ^{91}Zr: 10.10	54.2	^{90}Zr: 27.90, ^{91}Zr: 6.09
Mo	1900.0	^{95}Mo: 302.10, ^{98}Mo: 459.61	1088.7	^{95}Mo: 173.10, ^{98}Mo: 263.35
NIST SRM 664				
Si	660.0	^{29}Si: 30.92, ^{30}Si: 20.41	1276.6	^{29}Si: 59.81, ^{30}Si: 39.47
Cr	600.0	^{52}Cr: 502.73, ^{53}Cr: 57.01	626.9	^{52}Cr: 525.25, ^{53}Cr: 59.56
Zr	690.0	^{90}Zr: 355.01, ^{91}Zr: 77.42	410.9	^{90}Zr: 211.41, ^{91}Zr: 46.10
W	1000.0	^{184}W: 306.40, ^{186}W: 284.30	295.5	^{184}W: 90.54, ^{186}W: 84.01
Pb	240.0	^{206}Pb: 57.84, ^{207}Pb: 53.04	62.9	^{206}Pb: 15.17, ^{207}Pb: 13.91
NIST SRM 665				
B	1.3	^{10}B: 0.26, ^{11}B: 1.04	6.7	^{10}B: 1.34, ^{11}B: 5.37
S	59.0	^{32}S: 56.04, ^{34}S: 2.51	102.7	^{32}S: 97.51, ^{34}S: 4.36
Ti	6.0	^{46}Ti: 0.50, ^{47}Ti: 0.45, ^{49}Ti: 0.32	7.0	^{46}Ti: 0.58, ^{47}Ti: 0.52, ^{49}Ti: 0.38
Cr	70.0	^{52}Cr: 58.65, ^{53}Cr: 6.65	75.1	^{52}Cr: 62.93, ^{53}Cr: 7.14

Laser source characteristics

A laser pulse width of about 188 fs was measured at FWHM by using a sech^2 function as a fit function. Fig. 5 and 6 show the laser pulse profile measured with the autocorrelator system, and the pulse width stability measured with the autocorrelator

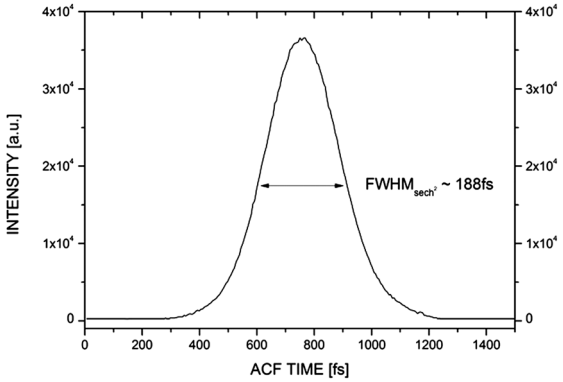

Fig. 5 A laser pulse profile measured with the autocorrelator (averaged over 8 single laser pulses). A laser pulse width of about 188 fs was determined at FWHM by using a sech^2 function as a fit function.

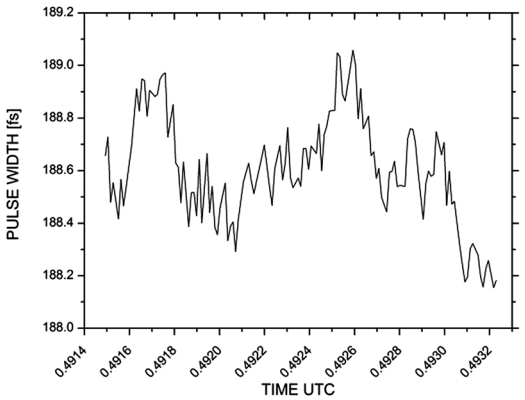

Fig. 6 Temporal stability of laser pulse duration over a time period of 150 s (150 000 single laser shots). Each data point corresponds to an average of 8 single laser pulse widths, measured and averaged with the autocorrelator.

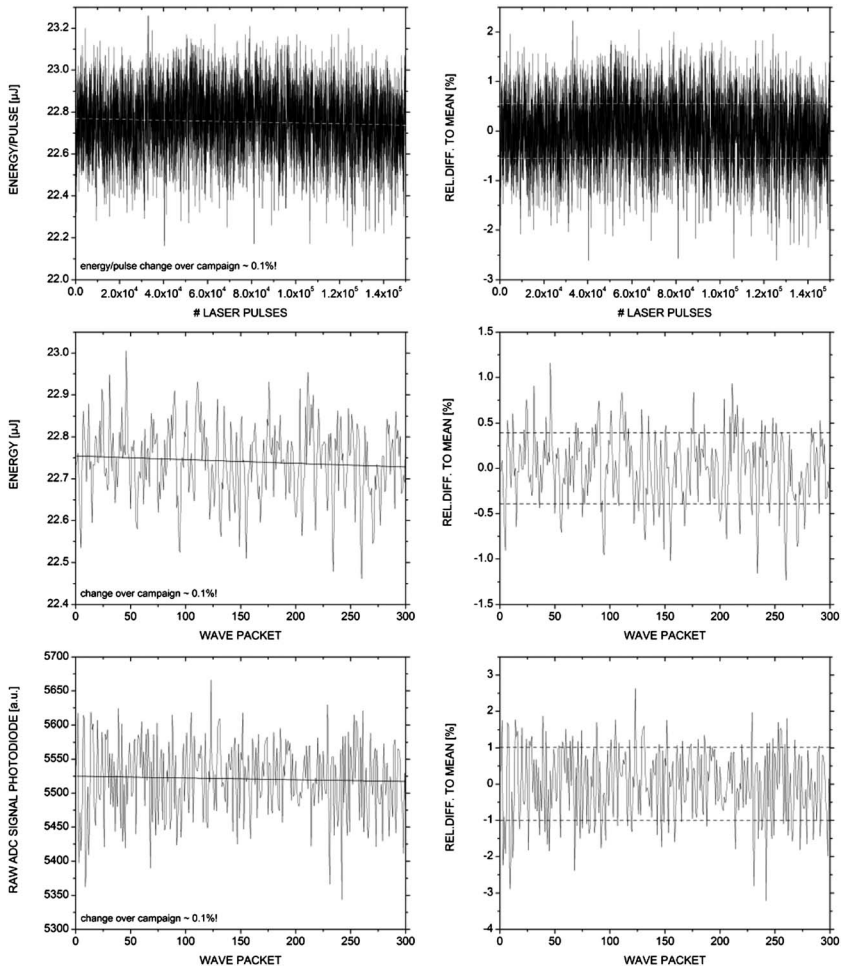

Fig. 7 Top panels: shot-to-shot laser fluctuations of 150 000 single laser shots, measured with a power/energy sensor (left panel), and standard deviation of fluctuations relative to the mean of about 6‰ is observed (right panel, dashed lines). Middle panels: 30 000 single laser shots taken from the data shown in the top panels. The single laser shots are averaged to files consisting of 100 single laser shots (300 files in total). Due to the average the standard deviation of the fluctuations relative to the mean is reduced to about 4‰. Bottom panels: 30 000 single laser shots measured with the ultrafast photodiode. Again, the single laser shots are averaged to files consisting of 100 single laser shots. Due to the slightly lower precision of the photodiode the standard deviation of the fluctuations relative to the mean is slightly increased to 1%.

during a time period of 150 s (150 000 single laser shots), respectively.

In Fig. 7 shot-to-shot laser intensity fluctuations are displayed. The straight lines in the left panels show the trend line through all the acquired and processed data. The dashed lines in the right panels correspond to the standard deviation of the fluctuations relative to the mean value.

In the top two panels of Fig. 7 the energy/pulse fluctuations (left) and the fluctuations relative to the mean of 150 000 single laser shots (corresponding to 150 s) are shown. While a power/energy meter console (LabMax-Top, Coherent, USA) in combination with a laser energy sensor (J-10MB-LE, Coherent, USA) was used to measure the energy of laser pulses, during the measurements the ultrafast photodiode was used to monitor the laser intensities. A high stability of laser pulse energy is observed with a relative change of pulse energy of 1‰, whereas shot-to-shot fluctuations relative to the mean showed a variation of about $\sigma = \pm 6‰$.

In the middle two panels similar data to those shown in the top two panels are displayed. However, these time averaged data files (wave packets of 100 single laser pulses) in a range of only 30 000 single laser pulse shots (300 files in total) are shown. Again and as expected, only a small variation of about 1‰ in energy/pulse is observed. Due to averaging of 100 single laser pulses the standard deviation of the fluctuations relative to the mean is decreased to about 4‰.

In the bottom two panels the fluctuations of 30 000 single laser shots are shown, measured with the photodiode, averaged to files consisting of 100 single laser shots (300 files in total). Only a small variation of laser intensity of about 1‰ is observed. However, by comparing these laser intensity fluctuations with the fluctuations observed in the previous measurement setup, where a Q-switched Nd:YAG ns-laser system was used,[22] the stability of the fs-laser system is observed to be significantly better. With the Nd:YAG laser system shot-to-shot laser intensity fluctuations of up to 40% were observed.[22]

Laser ablation characteristics

A sample of common steel material (AISI 316L) was used to study laser ablation craters that were produced after applying a

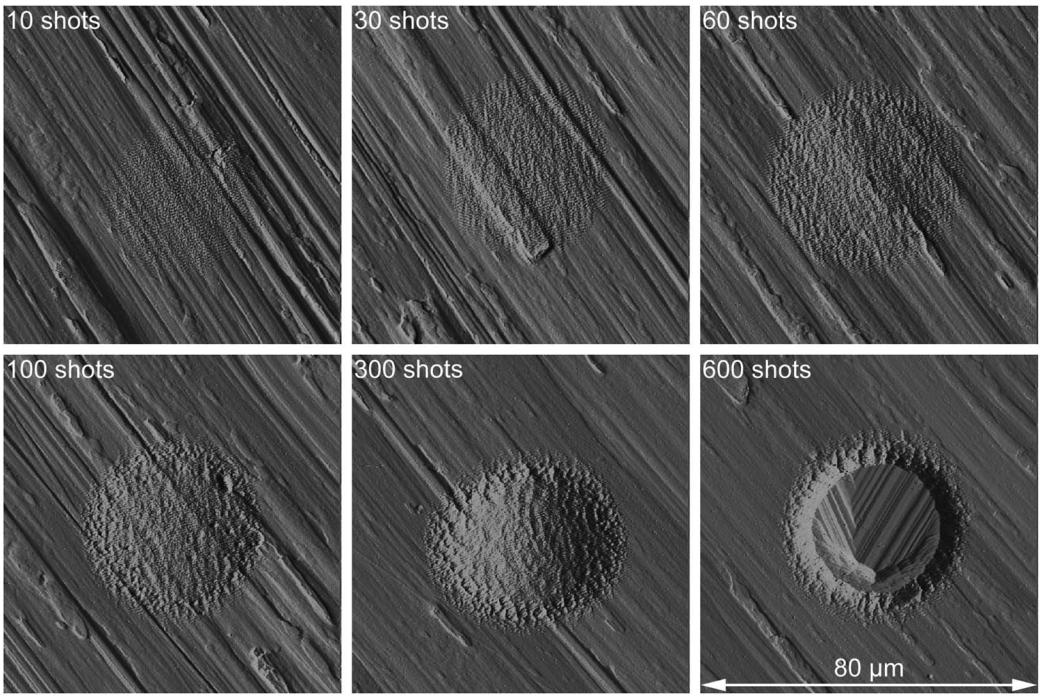

Fig. 8 AFM measurements of ablation craters built on an in-house prepared steel sample after 10, 30, 60, 100, 300 and 600 single laser shots (2.9 µJ per pulse). Crater diameters of about 40 µm are observed. In the first 60 single laser shots, ripples are observed.

different number of laser shots. The craters were analysed using an atomic force microscope, AFM (Bioscope II, Veeco, Germany). Sharp nitride lever probes with a nominal spring constant of 0.12 N m^{-1} and a nominal tip radius of 2 nm were used in the investigations. All measurements were performed in contact mode at ambient pressure and temperature. No additional liquids were used for the AFM measurements. In each measurement an area of 80 × 80 µm was investigated, with a spatial resolution of 512 × 512 pixels.

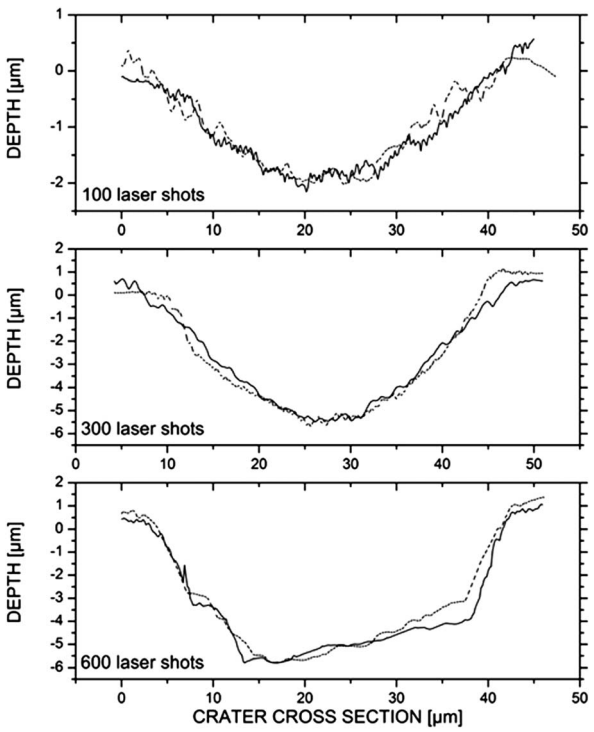

Fig. 9 AFM cross-sections of laser ablation pitch after 100, 300 and 600 single laser shots (2.9 µJ per pulse). Crater profiles after 100 and 300 single laser shots are in both *x*, *y* axes symmetric and have a Gaussian shape. After 600 laser shots the crater has steeper walls and shows a flatter crater bottom.

Fig. 8 shows AFM images of ablation craters excavated after 10, 30, 60, 100, 300 and 600 single laser shots (2.9 µJ per pulse). A crater diameter of about 40 µm is measured. Periodical microstructures, so-called ripples, are observed in AFM images of craters built after 10–60 single laser shots.[53,54] The orientation of these structures is perpendicular to the laser polarisation, which is in our case horizontal.[53,54]

Fig. 9 shows cross-sections of ablation craters formed after 100, 300 and 600 laser shots. The cross-sections for the craters built after 100 and 300 laser shots show a Gaussian profile and are symmetric in both axes (see also the corresponding craters in Fig. 8). This is slightly different regarding the crater formed after 600 laser shots. After 600 laser shots the crater has steeper walls and shows an almost flat crater bottom. In comparison with ablation craters produced with the ns-laser system,[22] the craters produced by the fs laser system are well structured and no rims around the crater are observed.[43]

fs-laser ablation ion source for space application

Present studies were accomplished by using a versatile Ti–Sapphire femtosecond laser system (Clark-MXR Inc., USA) as an ablation ion source. Laser parameters, such as energy per pulse, repetition rate, pulse duration, *etc.*, can be set easily *via* remote control by the user. However, it is unlikely that this

system can be used for space application because of its large size, weight and power consumption.

In the present report measurement campaigns were conducted at 1 kHz repetition rate, at 775 nm wavelength, ~190 fs pulse width, and in the energy per pulse range of about 1.1–6.2 μJ (laser ablation crater diameter: ~40 μm), corresponding to about 500–2700 GW cm^{-2}. Nevertheless, the laser focus spot can be reduced to several microns by the implementation of dedicated optics.[22] An increase of the spatial resolution is of considerable interest for space research and would allow the investigation of the chemical composition of micrometre-sized grains. An increase of the lateral resolution reduces significantly the requirements for the laser pulse energy to about 20–100 nJ (assuming a crater diameter of ~5 μm) which is necessary for stoichiometric ion production.

A miniature femtosecond fibre laser system with low power consumption for operation and significantly reduced weight is a suitable alternative to a Ti–Sapphire laser system, which is applied in this study. Nowadays, miniature ultra-short pulsed fibre systems are commercially available. One example would be the fs-fiber laser system from Femtolite Ultra systems, IMRA, USA. The following specifications of this system: wavelength of 810 ± 5 nm, average power ≥10 mW, pulse duration ≤110 fs, a total power consumption of less than 50 W, weight of <3 kg and total size of about 215 × 200 × 130 mm^3 are acceptable for implementation on planetary lander or rover.[55] Typically, such laser systems are operated at hundredths of kHz to MHz repetition rates, which can be too high for certain applications. By the implementation of optical shutter systems the repetition rate can be reduced to the desired frequency, at increased power consumption (tens of W).

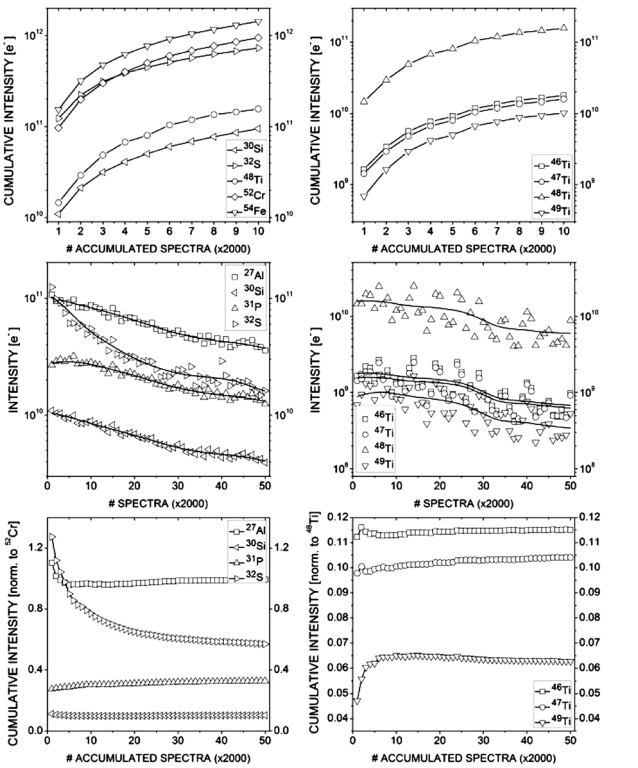

Fig. 10 Temporal signal stability of several investigated isotopes abundant in NIST SRM 661 during a single measurement campaign (see details in text). Top panels: cumulative peak intensities of different isotopes in the first 20 000 single laser shots. Middle panels: signal stability of different isotope peaks during the first 100 000 single laser shots. Bottom panels: cumulative peak intensities of different isotopes normalised to the intensity of ^{52}Cr in the first 100 000 single laser shots.

Results and discussion

Case study NIST SRM 661

Study on the number of accumulated spectra. Laser ablation/ionisation studies were conducted on a NIST SRM 661 sample to investigate the influence of a number of accumulations of individual spectra on the quantitative mass spectrometric analysis. A number of single laser shot spectra (total number of accumulation: 500 000) were collected at a constant laser irradiance of 1900 GW cm^{-2} (pulse energy ~4.4 μJ; laser beam diameter: Ø 40 μm) and repetition rate (1 kHz) from one single sample location.

Fig. 10 displays the temporal stability of the signal intensities (determined as integrated ion peak areas, middle panels), the cumulative intensities (upper panel), and the cumulative intensities normalised to the intensity of the ^{52}Cr mass peak (lower panels) of several isotope mass peaks observed during the measurements. In the top panel the cumulative peak intensities of ^{30}Si, ^{32}S, ^{48}Ti, *etc.* are shown that were observed after the accumulation of the first 20 000 single laser shot spectra. An almost similar rate of the cumulative sum of mass peak intensities is observed for most of the measured elements with an exception of the ^{32}S mass peak. A cumulative sum curve crossing is observed for ^{32}S and ^{52}Cr. In comparison to other isotopes, Sulphur shows a larger decrease of peak intensities (see the middle left panel). The signal variation and cumulative sum of peak intensities of Ti isotopes determined in the first 20 000 and 100 000 laser shot spectra, respectively, are shown in the right panels in Fig. 10. A relatively small intensity variation of mass peak intensities is observed during the first 10 000–16 000 laser shots with an exceptionally large signal decrease of the ^{32}S mass peak. Nevertheless, after these initial variations there are no significant peak intensity changes that are observed for most of the elements. Similar effects were observed in the previous studies conducted with a ns-laser ablation ion source.[31] The observation of relative mass peak intensity variation can be attributed to upper surface composition modification due to contact with atmospheric gases (*e.g.*, oxidation, contamination) and their influence on the ablation process (thermal–nonthermal behaviour). These effects contribute readily to elemental fractionation.[44]

Owing to the relative mass peak intensity variation for initial laser ablation pulses, the first 20 000 spectra are not considered for calculations of relative sensitivity coefficients (RSC), defined as measured abundance/quoted abundance.[28] This number was chosen by taking into account that the mass peak intensity of ^{32}S is observed to stabilise after ablation with so many laser pulses.

The dependence of the various measurement parameters on the number of accumulated spectra is shown in Fig. 11. The cumulative sum of peak intensities, cumulative sum of peak

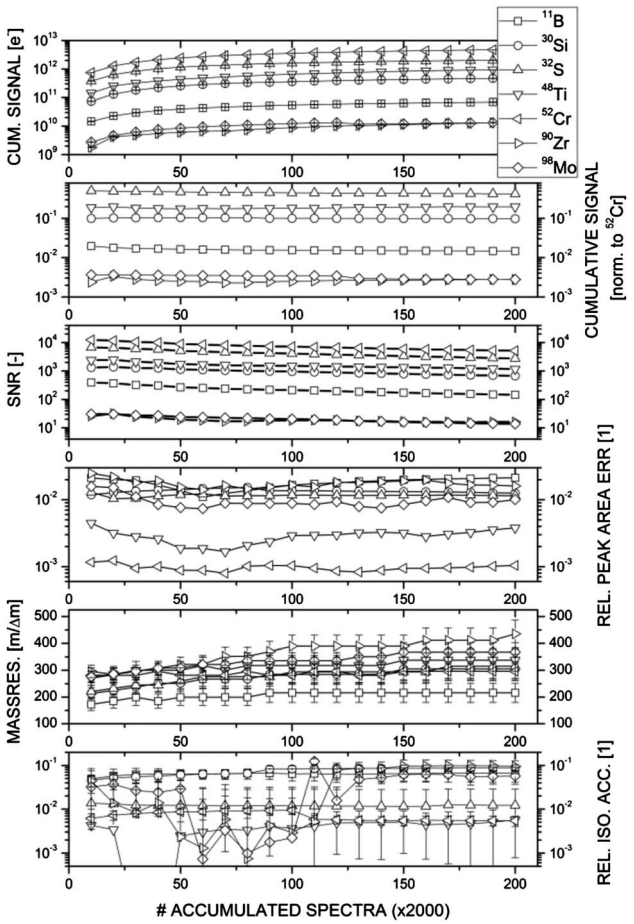

Fig. 11 The dependence of different measurement parameters, cumulative sum of peak intensities, cumulative sum of peak intensities normalised to the intensity of ^{52}Cr, SNR, relative peak area error, mass resolution, and relative isotope accuracy of measurement, on the number of spectral accumulations is shown. A single measurement campaign done on a NIST SRM 661 sample was used for this analysis (see details in text).

intensities normalised to the intensity of ^{52}Cr, SNR, relative peak area error, mass resolution $m/\Delta m$, relative isotope accuracy of measurement of different isotopes, *e.g.*, ^{11}B, ^{30}Si, ^{32}S, *etc.* are determined for up to 400 000 single shot spectra. The first 20 000 single laser shots were excluded.

No variation of relative cumulative sum is observed for most of the elements with an exception of Zr and Mo after 40 000 and 240 000, respectively. While the SNR decreases with the increase of the number of laser ablation shots, the mass resolution is relatively constant or increases slightly, in contrast to the measurements conducted with a ns-laser ablation ion source.[34] The lowest relative peak area errors, *e.g.*, mass peaks of ^{48}Ti and ^{52}Cr, are observed for the accumulation of about 100 000 to 140 000 single laser shot spectra. The measurements or relative isotope accuracies of measurements are observed to be constant for all elements with exception of ^{90}Zr and ^{98}Mo. Taking into account these observations, the first 100 000 spectra are chosen for the preparation of the quantitative compositional analysis.

Study on the influence of laser irradiance on the quantitative performance. To study the dependence of the relative measurement accuracies of isotope abundance on laser irradiance, mass spectrometric measurements were conducted for twelve different laser irradiances selected in the range of 500–2700 GW cm^{-2}, corresponding to an energy per pulse of about 1.1–6.2 μJ (with a laser beam diameter of Ø 40 μm). Each campaign was conducted on a fresh sample surface location. The spectra were obtained by accumulations of 100 000 single laser shot spectra, excluding the first 20 000 single laser shot spectra (see the previous section).

In Fig. 12 the dependence of several measurement parameters (signal intensity, SNR, relative peak area error, and mass resolution) of different isotopes, *e.g.*, ^{30}Si, ^{32}S, ^{52}Cr, *etc.*, on laser irradiance is shown. Similar to previous measurements conducted with a ns-laser ablation ion source,[34] we observe an increase of the signal intensity and SNR with increasing laser irradiance until these values stabilized and became independent of laser irradiance. We observed that for most of the elements, the signal becomes constant for laser irradiances larger than 1800 GW cm^{-2} (pulse energy of ~4.3 μJ; laser beam diameter Ø 40 μm). Due to the increased signal at increased irradiance a decreasing trend of relative peak area errors with increased irradiance is observed. By increasing the laser

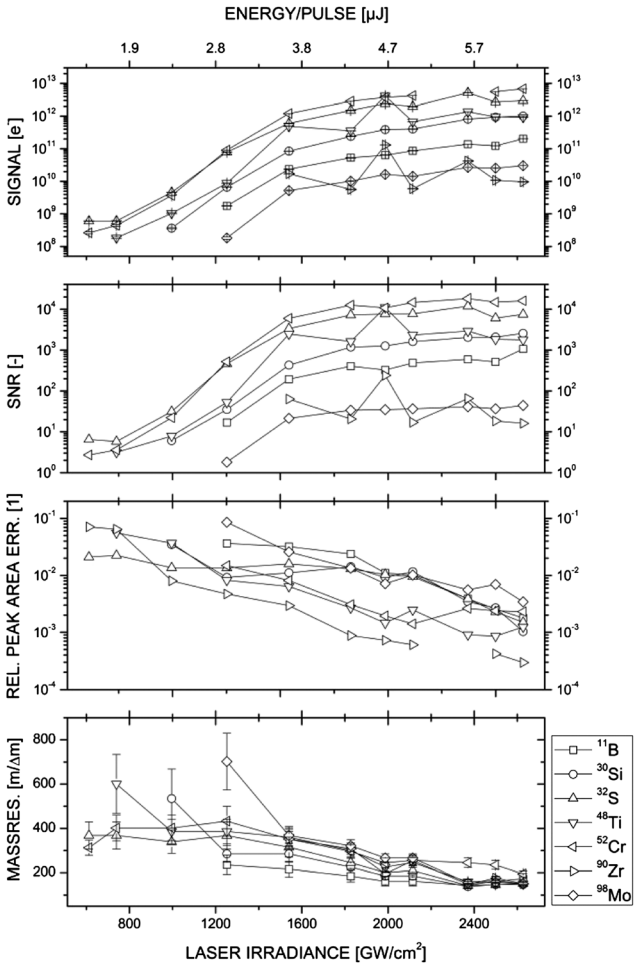

Fig. 12 The dependence of peak signal, SNR, relative peak area error, and mass resolution on the laser irradiances is shown. The laser irradiance campaign was conducted on a NIST SRM 661 sample.

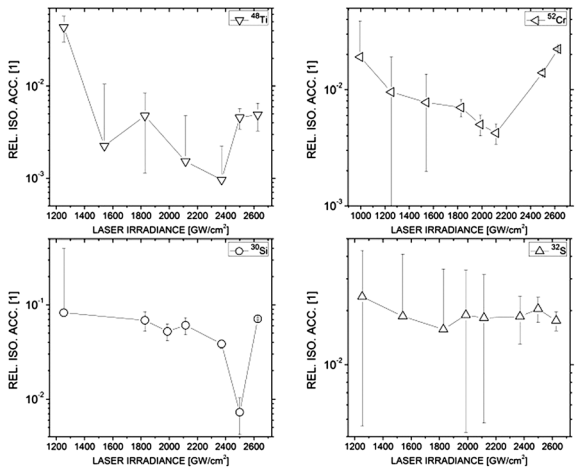

Fig. 13 The dependence of relative isotope accuracies of measurements on the applied laser irradiance is shown. The identical laser irradiance campaign conducted on NIST SRM 661 was used for this analysis (see Fig. 12).

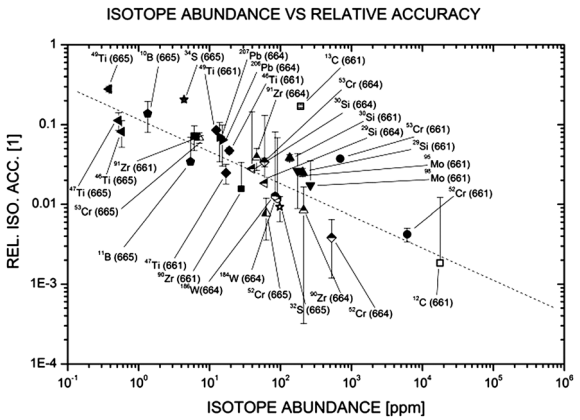

Fig. 14 Correlation between the abundance of an isotope and relative isotope accuracies of measurements. Isotope abundances are given in atomic fraction. An overview of the displayed isotopes, *e.g.* isotope abundances, corresponding NIST SRM samples, *etc.*, is given in Table 1.

irradiances the mass resolution is decreasing. The increase of laser irradiance causes an increase of the ablation rate and plasma plume temperature. Owing to a large number density of ions produced at increased laser irradiance, space charge effects, *e.g.*, surface charging and Coulombic repulsion become significant. At certain laser irradiance ion number densities are too large and exceed the focusing capacities of ion optics.

As noticed earlier,[34] a trend between ionisation thresholds and the boiling point[56] of the analysed elements and their isotopes (Cr(2671 °C), Ti(3287 °C), Si(3265 °C), B(4000 °C), Mo(4639 °C), and Zr(4406 °C)) is observed in these studies as well (data not shown); due to the very low boiling point sulphur is not included. A similar trend between ionisation threshold and melting point of different elements/isotopes was observed by Alcàntara *et al.* 2010 [57] by using an ns-laser system.

Fig. 13 shows the dependence of the relative isotope accuracies of measurements on the laser irradiance. For ^{30}Si and ^{32}S no trend of the relative isotope accuracies with increasing laser irradiance is observed within measurement accuracy. This is slightly different for ^{48}Ti and ^{52}Cr. Similar to previous observation in studies that applied a ns-laser ablation source[34] a broad minimum in the range of laser irradiances of about 1600–2400 GW cm^{-2} is observed where the best relative isotope accuracies of measurements are obtained.[34]

Isotope abundance *versus* measurement accuracy

In Fig. 14 the correlation between isotope abundances (in atomic fraction) and the relative isotope accuracies of measurements for many different isotopes, measured in the NIST samples SRM 661, 664, and 664, is shown. The similar measurement procedure discussed for the NIST SRM 661 case study was used to investigate elements/isotopes abundant in NIST SRM 664 and 665. An overview of the investigated isotopes, *e.g.* isotope abundances, corresponding NIST SRM samples, *etc.*, can be found in Table 1.

An increase of measurement accuracy with increase of isotope abundance is observed as expected. For isotope abundances in the range of about 100 ppm a measurement accuracy of 1% and better can be achieved. A similar correlation was observed in previous measurements performed with a ns-laser ablation ion source.[34] However, the accuracy of the current measurements is larger and the measured values lie closer to the trend line. For example, the measurement accuracy at 100 ppb abundance is improved in these studies by a factor of about 2–3 compared to the previous investigations and is determined at about 25% error.[34]

The trend between isotope abundances and relative isotope accuracies of measurements shows a slope of about −0.5 in log/log-space. This observation can directly be correlated with the trend between the relative ion peak area error, defined as $\delta A/A$, and SNR, which is a composite of relative statistical error, relative background error, and relative peak area error of integration of ion signal.[52] In comparison with the relative statistical error and relative background error the relative peak area error by Simpson integration is by 2–3 decades more significant, and shows a trend between the relative peak area error and SNR of about −0.5 in log/log-space.[52] To improve the overall performance of relative isotope accuracy of measurement the SNR has to be improved by the implementation of a more sensitive detection system and less noisy acquisition cards with higher sampling rate. With increased SNR of detected ion mass peaks the relative ion peak area error introduced by integration decreases and hence, the relative isotope accuracy of measurement can be increased. With the present setup (detector gain of ~10^6 to 10^7, 4.8 μJ per pulse) one single ^{11}B ion (NIST SRM 665 sample) with a weight fraction ~1 ppm (Table 1) is detected statistically per 1 laser shot. More details can be found in the report by Meyer, 2013.[52]

Recently, a few instruments were designed for *in situ* geochronology of solid planetary surface material. The potassium–argon laser experiment (KArLE)[20] or the instrumental suite combining XRS and GAP[17–19] were designed for geochronology with the K–Ar dating method. Another instrument, such as the laser desorption resonance ionisation mass spectrometer, LDRIMS, is based on the measurements of Rb and Sr

isotopes.[21] In comparison with these instruments, the design and measurement principle of the miniature reflectron time-of-flight LMS system is robust and simple, and it offers a high dynamic range of at least eight orders of magnitude. A current detection limit on metallic and non-metallic elements is determined at a few ppb level. A more detailed discussion on the performance of LMS for the *in situ* geochronology can be found in an earlier publication.[34]

Performance comparison between ns- and fs-measurements

A fs-laser ablation ion source is clearly advantageous to that of a ns-source, which we applied in previous studies. In addition to a long term stability of the measurement parameters presented in the previous sections, the improvement of spectral quality and detection efficiency of all ions was achieved. Fig. 15 displays sections of mass spectra within the m/q range of about 27–34 of NIST SRM 661 obtained by the application of the femtosecond and ns-laser ablation ion sources. Both spectra were obtained by accumulation of 100 000 accumulated single shot spectra. The top spectrum is obtained by using the previously discussed ns-laser ($\lambda = 266$ nm, $\tau \sim 3$ ns, Ø 20 μm, 20 Hz repetition rate) system for ablation and ionisation of the sample material.[34] The spectrum was recorded at a laser irradiance of about 0.5 GW cm^{-2}. The bottom section is conducted by using the present fs-laser system ($\lambda = 775$ nm, $\tau \sim 190$ fs, Ø 40 μm, 1 kHz repetition rate) at a laser irradiance of about 1900 GW cm^{-2}. Elemental and isotope abundances displayed in both panels are given in atomic fractions.

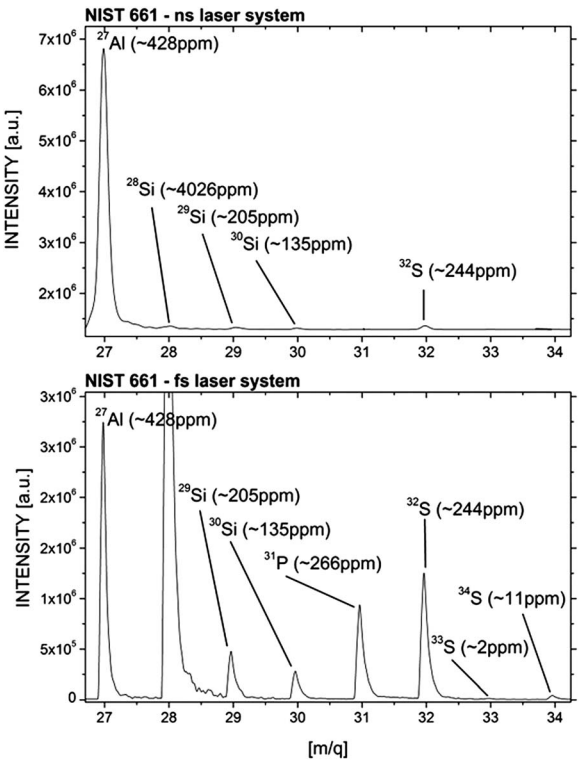

Fig. 15 Comparison between sections of mass spectra within m/q of about 27–34 of the NIST SRM 661 sample, measured with the previous ns- and present fs-laser ablation ion sources. Each spectrum is an accumulation of 100 000 single laser shot spectra.

Table 2 Comparison between relative sensitivity coefficients (RSC) using the ns-laser at IR wavelength,[28] ns-system at UV, and fs-laser system at IR radiation. In the last row the corresponding ionisation potentials of the listed elements are given. The listed RSC values result from the measurements conducted on NIST SRM 661 samples (more details in text)

	C	Si	P	S	V
ns-system (IR)	1.3×10^{-3}	1.6×10^{-2}	—	—	1.7
ns-system (UV)	2×10^{-4}	2×10^{-2}	3×10^{-2}	5×10^{-2}	3.2
fs-system (IR)	0.90	1.04	1.10	1.16	0.9
IP [eV]	11.260	8.151	10.486	10.316	6.82

The appearance of these two spectra is significantly different. The detection efficiency for non-metallic elements is much lower than for metals when the ns-laser ablation ion source is applied (top panel). The mass peak of ^{27}Al (~428 ppm) is more intense than that of ^{28}Si (~4026 ppm) or ^{32}S. The measurement conducted by using the fs-laser ablation ion source shows correct intensities of the relevant mass peaks in accord with the element (isotope) abundances of these species in a sample (bottom panel). The comparison of the relative abundance ratios determined from the measurement and compared to the NIST quoted values shows good agreement between the measured and quoted values. Relative sensitivity coefficients of elements are shown in Table 2 along with a subset of RSC values of relevant elements and the corresponding ionisation potentials (IP, last row) obtained using different laser-systems on a NIST SRM 661 sample. In the first row RSC values from measurements conducted with a ns-laser system at IR wavelength ($\lambda = 1064$ nm, $\tau \sim 4$ ns, Ø 10 μm, 20 Hz repetition rate) are listed; in the second row values obtained using the ns-laser system at UV,[22] and in the third row the RSC values obtained using the present fs-laser system. More details about the ns-laser setup used at IR radiation and the listed RSC values can be found in an earlier publication.[28] While the ns-RSC values of the listed elements are in the range of 10^{-4} to 2, if even available (see IR), the RSC values obtained using the present fs-laser system are close to 1. The results of these studies are of considerable importance for development of standard-less instruments that can be used for the elemental analysis of various types of solid samples and capable of conducting accurate isotope analysis.

Conclusion and outlook

Mass spectrometric analysis of elemental and isotopic composition of several NIST standard reference materials is performed by a miniature laser ablation/ionisation reflectron-type time-of-flight mass spectrometer designed for *in situ* space research using an fs-laser ablation ion source. The studies indicate that the accurate quantitative analysis of elemental and isotope compositions can be performed by controlling laser irradiance and the number of accumulations of single laser shot spectra. These experimental conditions are established *via* systematic

parametric investigation of the influence of laser irradiance on measured elemental and isotopic compositions.

The studies show that measurements on the isotope composition can be conducted within measurement accuracy at the per mill level for isotope concentrations larger than 100 ppm. The measurement accuracy is degraded with lower elemental/isotopic concentration in a sample material. For elements and isotopes with abundances below 100 ppm the relative measurement accuracy drops to the per cent level. For isotopes with sample concentrations of ~100 ppb, an increase of the measurement accuracy by a factor of 2–3 compared with studies conducted with an ns-laser ablation ion source is observed.

Further improvements of accuracy of the studies can be made by improvements of detection sensitivity, which is found to be currently the limiting factor.

The mass spectrometric studies indicate superior performance of the instrument for the elemental analysis while a fs-laser ablation ion source is applied. A similar detection efficiency of metallic and non-metallic elements is observed and relative sensitivity coefficients determined from the mass spectrometric analysis of investigated standards were close to one. Thermal effects, sample damage and additional laser-plasma interaction are negligible or not present during fs-laser ablation in contrast to that of the ns-laser ion source. Their absence together with superior characteristics of the fs-laser beam account for the substantial improvement of the accuracy of elemental analysis. Further studies are planned to establish the influence of the other characteristics of the fs-laser ablation source as well as material composition (matrix effects) on the accuracy of the elemental analyses. The results are of considerable importance for the development of standard-less instrumentation for the compositional (elemental and isotopic) investigation of solid material on planetary surfaces.

Acknowledgements

Harry Mischler, Jürg Jost, and Daniele Piazza are acknowledged for their continuous support and a number of improvements made to the instrument over the years. Dominik Marti and Martin Frenz from the Applied Institute of Physics, University of Bern are acknowledged for their help during the AFM measurements. This work is supported by the Swiss National Science Foundation.

Notes and references

1 U. Rohner, J. A. Whitby and P. Wurz, *Meas. Sci. Technol.*, 2003, **14**, 2159–2164.
2 U. Rohner, J. A. Whitby, P. Wurz and S. Barabash, *Rev. Sci. Instrum.*, 2004, **75**, 1314–1322.
3 W. B. Brinckerhoff, G. G. Managadze, R. W. McEntire, A. F. Cheng and W. J. Green, *Rev. Sci. Instrum.*, 2000, **71**, 536–545.
4 G. G. Managadze, P. Wurz, R. Z. Sagdeev, A. E. Chumikov, M. Tuley, M. Yakovleva, N. G. Managadze and A. L. Bondarenko, *Sol. Syst. Res.*, 2010, **44**, 376–384.
5 J. Chela-Flores and N. Kumar, *Int. J. Astrobiol.*, 2008, **7**, 263–269.
6 I. N. Tolstikhin and J. D. Kramers, *The evolution of matter*, Cambridge University Press, Cambridge, 2008.
7 J. Blichert-Toft, B. Zanda, D. S. Ebel and F. Albarède, *Earth Planet. Sci. Lett.*, 2010, **300**, 152–163.
8 A. Bouvier and M. Wadhwa, *Nat. Geosci.*, 2010, **3**, 637–641.
9 H. Y. McSween and G. Huss, *Cosmochemistry*, Cambridge University Press, Cambridge, 2010.
10 I. P. Wright, S. J. Barber, G. H. Morgan, A. D. Morse, S. Sheridan, D. J. Andrews, J. Maynard, D. Yau, S. T. Evans, M. R. Leese, J. C. Zarnecki, B. J. Kent, N. R. Waltham, M. S. Whalley, S. Heys, D. L. Drummond, R. L. Edeson, E. C. Sawyer, R. F. Turner and C. T. Pillinger, *Space Sci. Rev.*, 2007, **128**, 363–381.
11 J. F. J. Todd, S. J. Barber, I. P. Wright, G. H. Morgan, A. D. Morse, S. Sheridan, M. R. Leese, J. Maynard, S. T. Evans, C. T. Pillinger, D. L. Drummond, S. C. Heys, S. E. Huq, B. J. Kent, E. C. Sawyer, M. S. Whalley and N. R. Waltham, *J. Mass Spectrom.*, 2007, **42**, 1–10.
12 E. K. Gibson, C. T. Pillinger and L. J. Waugh, *Earth, Moon, Planets*, 2010, **107**, 25–42.
13 D. Pullan, M. R. Sims, I. P. Wright, C. T. Pillinger and R. Trautner, *Mars Express: the scientific payload, ESA SP-1240, 165–204*, ed. A. Wilson, ESA Publications Division, Noordwijk, Netherlands, ISBN 92-9092-556-6, 2004.
14 M. P. Sinha, E. L. Neidholdt, J. Hurowitz, W. Sturhahn, B. Beard and M. H. Hecht, *Rev. Sci. Instrum.*, 2011, **82**, 094102.
15 H. Y. McSween Jr, R. L. McNutt Jr and T. H. Prettyman, *Proc. Natl. Acad. Sci. U. S. A.*, 2011, **108**, 19177–19182.
16 M. Tulej, A. Riedo, M. Neuland, S. Meyer and P. Wurz, Elemental analysis of planetary surfaces: overview of concepts, instrumentation and results, *Appl. Spectrosc. Rev.*, 2013, submitted.
17 D. L. Talboys, S. Barber, J. C. Bridges, S. P. Kelley, D. Pullan, A. B. Verchovsky, G. Butcher, A. Fazel, G. W. Fraser, C. T. Pillinger, M. R. Sims and I. P. Wright, *Planet. Space Sci.*, 2009, **57**, 1237–1245.
18 R. Rieder, T. Economou, H. Wänke, A. Turkevich, J. Crisp, J. Brückner, G. Dreibus and H. Y. McSween Jr, *Science*, 1997, **278**, 1771–1774.
19 I. P. Wright, M. R. Sims and C. T. Pillinger, *Acta Astronaut.*, 2003, **52**, 219–225.
20 B. A. Cohen, Development of the potassium-argon laser experiment (KARLE) instrument for *in situ* Geochronology, in *43rd Lunar Planet. Sci. Conf.*, 2012, Abstract Nr. 1267.
21 E. Hand, *Nature*, 2012, **487**, 422–425.
22 A. Riedo, A. Bieler, M. Neuland, M. Tulej and P. Wurz, *J. Mass Spectrom.*, 2013, **48**, 1–15, DOI: 10.1002/jms.3104.
23 J. S. Becker, *Inorganic mass spectrometry – Principles and Applications*, John Wiley & Sons Ltd, England, 2007.
24 Q. Yu, Z. Cao, L. Li, B. Yan, W. Hang, J. He and B. Huang, *Anal. Chem.*, 2009, **81**, 4343–4348.
25 F. Caridi, L. Torrisi, A. Borrielli and G. Mondio, *Radiat. Eff. Defects Solids*, 2010, **165**, 668–680.
26 J. S. Becker and H. J. Dietze, *Int. J. Mass Spectrom.*, 2000, **197**, 1–35.

27 J. S. Becker, *J. Anal. At. Spectrom.*, 2002, **17**, 1172–1185.
28 M. Tulej, M. Iakovleva, I. Leya and P. Wurz, *Anal. Bioanal. Chem.*, 2011, **399**, 2185–2200.
29 Y. Lin, Q. Yu, W. Hang and B. Huang, *Spectrochim. Acta, Part B*, 2010, **65**, 871–883.
30 Q. Yu, R. Huang, W. Hang, J. He and B. Huang, *TrAC, Trends Anal. Chem.*, 2009, **28**, 1174–1185.
31 M. Tulej, A. Riedo, M. Iakovleva and P. Wurz, *Int. J. Spectrosc.*, 2012, DOI: 10.1155/2012/234949.
32 M. B. Neuland, S. Meyer, A. Riedo, M. Tulej, P. Wurz and K. Mezger, Probing the Allende Meteorite with LMS, a Miniature Laser-Ablation Mass Analyser for Space Application, *Planet. Space Sci.*, 2013, submitted.
33 A. Riedo, A. Bieler, M. Neuland, M. Tulej and P. Wurz, *J. Mass Spectrom.*, 2013, **48**, 1–15, DOI: 10.1002/jms.3157.
34 A. Riedo, S. Meyer, B. Heredia, M. Neuland, A. Bieler, M. Tulej, I. Leya, M. Iakovleva, K. Mezger and P. Wurz, Highly accurate isotope composition measurements by a miniature laser ablation mass spectrometer designed for *in situ* investigations on planetary surfaces, *Planet. Space Sci.*, 2013, submitted.
35 R. E. Russo, X. Mao, H. Liu, J. Gonzales and S. S. Mao, *Talanta*, 2002, **57**, 425–451.
36 R. Hergenröder, O. Samek and V. Hommes, *Mass Spectrom. Rev.*, 2006, **25**, 551–572.
37 Y. Lin, Q. Yu, W. Hang and B. Huang, *Spectrochim. Acta, Part B*, 2010, **65**, 871–883.
38 R. Huang, Q. Yu, L. Li, Y. Lin, W. Hang, J. He and B. Huang, *Mass Spectrom. Rev.*, 2011, **30**, 1256–1268.
39 L. Li, B. Zhang, R. Huang, W. Hang, J. He and B. Huang, *Anal.Chem.*, 2010, **82**, 1949–1953.
40 Q. Yu, R. Huang, L. Li, L. Lin, W. Hang, J. He and B. Huang, *Anal. Chem.*, 2009, **81**, 4343–4348.
41 Q. Yu, L. Chen, R. Huang, W. Hang, J. He and B. Huang, *TrAC, Trends Anal. Chem.*, 2009, **28**, 1174–1185.
42 A. A. Sysoev and A. A. Sysoev, *Eur. J. Mass Spectrom.*, 2002, **8**, 213–232.
43 R. E. Russo, X. Mao, J. J. Gonzales and J. Yoo, *Spectroscopy*, 2013, **28**, 24–39.
44 R. E. Russo, X. Mao, J. J. Gonazales and S. S. Mao, *J. Anal. At. Spectrom.*, 2002, **17**, 1072–1075.
45 J. J. Gonzales, A. Fernandez, D. Oropeza, X. Mao and R. E. Russo, *Spectrochim. Acta, Part B*, 2008, **63**, 277–286.
46 X. Zeng, X. L. Mao, R. Greif and R. E. Russo, *Appl. Phys. A: Mater. Sci. Process.*, 2005, **80**, 237–241.
47 J. González, S. H. Dundas, C. Y. Liu, X. Mao and R. E. Russo, *J. Anal. At. Spectrom.*, 2006, **21**, 778–784.
48 D. J. Hwang, H. Jeon, C. P. Grigoropoulos, J. Yoo and R. E. Russo, *Appl. Phys. Lett.*, 2007, **91**, 251118.
49 A. Bieler, K. Altwegg, L. Hofer, A. Jäckel, A. Riedo, T. Sémon, P. Wahlström and P. Wurz, *J. Mass Spectrom.*, 2011, **46**, 1143–1151.
50 A. Bieler, Design of a novel time of flight mass spectrometer and practical application of computer optimization to the development and tuning of mass spectrometers, PhD Thesis, University of Bern, Switzerland, 2012.
51 R. B. Marinenko, K. F. J. Heinrich and F. C. Ruegg, *Standard Reference Materials: Micro-Homogeneity Studies of NBS Standard Reference Materials, NBS Research Materials, and Other Related Samples, Special Publication 260–65*, National Bureau of Standards, Washington DC, 1979.
52 S. Meyer, Development of fully automated and high precise data analysis for a miniaturized laser-ablation mass spectrometer, MSc. Thesis, University of Bern, Switzerland, 2013.
53 B. Raillard, L. Gouton, E. Ramos-Moore, S. Grandtyll, F. Müller and F. Mücklich, *Surf. Coat. Technol.*, 2012, **207**, 102–109.
54 M. Huang, F. Zhao, Y. Cheng, N. Xu and Z. Xu, *ACS Nano*, 2009, **3**, 4062–4070.
55 J. P. Grotzinger, J. Crisp, A. R. Vasavada, R. C. Anderson, C. J. Baker, R. Barry, D. F. Blake, P. Conrad, K. S. Edgett, B. Ferdowski, R. Gellert, J. B. Gilbert, M. Golombek, J. Gómez-Elvira, D. M. Hassler, L. Jandura, M. Litvak, P. Mahaffy, J. Maki, M. Meyer, M. C. Malin, I. Mitrofanov, J. J. Simmonds, D. Vaniman, R. V. Welch and R. C. Wiens, *Space Sci. Rev.*, 2012, **170**, 5–56.
56 CRC Handbook of Chemistry and Physics, 2012–2013, 93rd edn, http://www.hbcpnetbase.com, accessed March 2013.
57 J. F. Alcántara, J. M. Vadillo and J. J. Laserna, *J. Anal. At. Spectrom.*, 2010, **25**, 1424–1431.